

PAPER • OPEN ACCESS

Air temperature sensors: dependence of radiative errors on sensor diameter in precision metrology and meteorology

To cite this article: Michael de Podesta et al 2018 Metrologia 55 229

View the article online for updates and enhancements.

You may also like

- Influence of Meteorological Variables on UHF Radio Signal: Recent Findings for EBS, Benin City, South-South, Nigeria K.E. Ukhurebor and O.J. Umukoro
- Effects of changes in land use on the diurnal temperature range: a long-term data analysis
 Kazuki Ueno and Shunji Ohta
- Thermal metrology for climate: a review of projects, activities and open issues
 Andrea Merlone

Recent citations

- A review of state-of-the-art 1D length scale calibration instruments
 Tim Coveney
- Air temperature measurement challenges in precision metrology M de Podesta et al

Metrologia 55 (2018) 229-244

Air temperature sensors: dependence of radiative errors on sensor diameter in precision metrology and meteorology

Michael de Podesta[®], Stephanie Bell and Robin Underwood

National Physical Laboratory, Hampton Road, Teddington, TW11 0LW, United Kingdom

E-mail: michael.depodesta@npl.co.uk

Received 11 October 2017, revised 12 January 2018 Accepted for publication 24 January 2018 Published 28 February 2018



Abstract

In both meteorological and metrological applications, it is well known that air temperature sensors are susceptible to radiative errors. However, it is not widely known that the radiative error measured by an air temperature sensor in flowing air depends upon the sensor diameter, with smaller sensors reporting values closer to true air temperature. This is not a transient effect related to sensor heat capacity, but a fluid-dynamical effect arising from heat and mass flow in cylindrical geometries. This result has been known historically and is in meteorology text books. However, its significance does not appear to be widely appreciated and, as a consequence, air temperature can be—and probably is being—widely mis-estimated.

In this paper, we first review prior descriptions of the 'sensor size' effect from the metrological and meteorological literature. We develop a heat transfer model to describe the process for cylindrical sensors, and evaluate the predicted temperature error for a range of sensor sizes and air speeds. We compare these predictions with published predictions and measurements. We report measurements demonstrating this effect in two laboratories at NPL in which the air flow and temperature are exceptionally closely controlled. The results are consistent with the heat-transfer model, and show that the air temperature error is proportional to the square root of the sensor diameter and that, even under good laboratory conditions, it can exceed 0.1 °C for a 6 mm diameter sensor.

We then consider the implications of this result. In metrological applications, errors of the order of 0.1 °C are significant, representing limiting uncertainties in dimensional and mass measurements. In meteorological applications, radiative errors can easily be much larger. But in both cases, an understanding of the diameter dependence allows assessment and correction of the radiative error using a multi-sensor technique.

Keywords: air temperature, meteorology, errors, sensors, metrology

(Some figures may appear in colour only in the online journal)

1. Introduction

1.1. General

Air temperature measurements are among the most common measurements made on Earth. In both meteorological and

Original content from this work may be used under the terms of the Creative Commons Attribution 3.0 licence. Any further distribution of this work must maintain attribution to the author(s) and the title of the work, journal citation and DOI.

metrological applications, it is well known that temperature sensors are susceptible to radiative errors, both from direct irradiation by the Sun and lighting sources, and also from thermal sources such as the walls of a room, an enclosure or a human body. However, without auxiliary measurements, it is not possible to know whether or not a particular temperature measurement has been affected.

The work reported here began in 2013 as part of an attempt to improve the calibration of air temperature sensors at NPL.

We undertook a series of experiments using a small wind tunnel and a variety of temperature sensors. But being unaware of the sensor-size and air speed dependence effects which we describe in this paper, we were unable to fully understand our results at that time. In 2017 we re-visited the problem using an acoustic thermometer which makes non-contact measurements of air temperature [1, 2]. At this point the problem with conventional air temperature measurements became apparent.

The key insight reported in this paper is that the radiative error for an air temperature sensor in flowing air depends upon the sensor diameter and air speed, with smaller sensors and higher air speeds yielding values closer to true air temperature. This is not a transient effect related to the sensor heat capacity, but a fluid-dynamical effect arising from heat and mass flow in cylindrical geometries in the steady state.

This is not a new insight. In his 1968 paper, Daniels [3] refers to papers describing the effect which date back to 1815. However, even though the result is in meteorology text books [4], it does not appear to be widely known amongst metrologists, and as a consequence air temperature can be—and probably is being—widely mis-estimated.

In this paper we begin with a sampling of the metrological (section 1.2) and meteorological (section 1.3) literature. We highlight papers which refer to the effects in this paper, and also papers in which there is surprisingly no mention of the effects. In section 2, we describe a heat-transfer model and compare it with the published data. In section 3, we describe measurements made within our closely controlled laboratories and compare our model with the results. Finally, in section 4 we discuss the implications of the insights described here for precision metrology and for meteorology.

1.2. Metrology

In metrological applications, air temperature is required in the estimation of the refractive index for dimensional measurements and in the estimation of air density for buoyancy corrections in precision weighing. In addition, flowing air within laboratories and climatic chambers is used to control the temperature of the objects under study. In these applications, errors of the order of 0.1 °C are significant, representing limiting uncertainties in their respective fields.

In the temperature-stabilised laboratories and climatic chambers in which these activities are carried out, it might seem that radiative errors would be small or negligible. Furthermore, standard texts on precision temperature measurements have relatively few recommendations regarding radiative errors in air temperature measurement.

Nicholas and White [5] point out the 'insidious nature' of radiative errors, especially when the thermal contact between the sensor and the object of interest is weak. However, if the source of the irradiation cannot be removed, their recommendation is that a radiation shield should be used. They then highlight problems with the use of radiation shields. Quinn [6] and Bentley [7] spare only a few words on air temperature measurement, concentrating on the difficulties of aeronautical measurements. Similarly, the ASTM manual on *The Use of*

Thermocouples in Temperature Measurement [8] refers to the time lag and temperature error inside a thermowell used to measure fluid temperatures, but does not draw attention to the effect of sensor diameter. Bentley [9] and Michalski et al [10] do draw attention to the need to assess the radiative balance between the sensor and its environment when measuring gas temperatures. Bentley states that the heat transfer coefficient depends on the sensor 'shape, roughness and inclination', but does not mention size. The discussion of the problem is otherwise extensive, but neither he nor Michalski suggest any diameter dependence.

In a comparison of air temperature calibration procedures, Heinonen *et al* [11] record the diameter of the probes used, deliberately use probes with different emissivities, and analyse their results to study the effects of emissivity. However, they do not analyse the dependence of radiative errors on diameter. Friederici and Tegeler [12] are quoted in [11] as discussing the potential errors arising from thermal radiation in climatic chambers. In [12] they highlight the fact that the heat transfer coefficient of a thermometer in air depends on its diameter, a prediction they confirm qualitatively.

Friederici and Tegeler's main concern is with the emissivity of sensor surfaces. However, they raise a profound question in the final section of their paper regarding the meaning of the phrase 'the temperature of a climatic chamber'. They ask whether this is (a) the temperature of a test body placed at a particular location in the chamber or (b) the temperature of the air at that location in the chamber. The implication of their question is that options (a) and (b) will result in different answers. In the present work we are really evaluating the relationship between cases (a) and (b) for a specific form of test object, namely a cylindrical thermometer. Friederici and Tegeler suggest four different methods for assessing the radiation effect: (i) measuring using two thermometers with widely differing emissivity; (ii) measuring with and without a radiation shield; (iii) measuring with a low emissivity thermometer and measuring the wall temperature; and (iv) neglecting the radiation error for temperatures close to ambient. They do not include a fifth option, which we describe here, namely studying the diameter dependence of the thermometer reading.

Both Incropera and De Witt [13] and Çengal and Ghajar [14] include a detailed description of the size dependence of the heat transfer coefficient for air flowing past a cylinder, a situation sometimes described as 'forced convection'. The key insight of their analysis is the understanding that the heat transfer between the gas and the cylinder takes place in a boundary layer whose dimensions depend on the thermal conductivity, heat capacity, viscosity, speed and density of the air. For cylinders with a diameter much larger than this boundary layer, the flowing air in contact with the cylinder surface rapidly equilibrates to the temperature of the cylinder surface, and so heat transfer is relatively weak. As the cylinder diameter is reduced towards the boundary layer thickness, the heat transfer per unit area becomes proportionately more effective. For air at typical laboratory conditions flowing at speeds between 0.1 m s⁻¹ and 1 m s⁻¹, this boundary layer is of the order of millimetres to centimetres in thickness, and thus heat

transfer *per unit area* naturally exhibits a size dependence, being higher for smaller objects.

1.3. Meteorology

This short survey of the meteorological literature on the subject is not intended to be exhaustive. Rather our aim is to illustrate the long-standing appreciation of the problem within meteorology.

In meteorological applications, air temperature is the most commonly reported measurand, and measurements are known to be subject to radiative errors even when made within thermometer screens, such as Stevenson screens, radiation baffles and aspirated enclosures. Many textbooks, e.g. Burt [15], discuss the character of the errors caused and their correlation with wind speed.

Extensive research on air thermometry was carried out in the 1950s and 1960s, particularly with regard to measurements in the upper atmosphere using sensors borne on balloons and parachutes.

In their 1960 paper on *The Measurement of Atmospheric Temperature*, Ney, Maas and Huch [16] describe the thermal problem of an irradiated object (a temperature sensor) in air travelling at speed through the atmosphere from the ground to altitudes with pressures of 100 hPa. The paper has a particularly insightful introduction, highlighting the mechanisms of heat transfer at different pressures, and the origin of the diameter dependence of the heat transfer with the air.

Daniels [3] uses similar insights to Ney Mass and Huch, and describes the measurement of air temperature in meteorological exposures without a screen, using a Radiation Compensating Thermocouple [3]. The paper includes a thorough bibliography reporting air temperature studies as early as 1815 [17]. Daniels describes the emergence of the insight through the 19th Century that the temperature error in gas temperature measurements depends on the diameter of the probe. He reports that in 1898 Waggenner [18] described the use of thermometer readings from multiple thermocouples of different diameters to determine the temperature of flames, and it is this principle that Daniels uses to devise his Radiation Compensating Thermocouple. The device is a composite of three thermocouples in which the ratios of the wire diameters are chosen such that the radiation error from the larger diameter thermocouple wire is cancelled by the sum of the errors from two smaller diameter thermocouples wired in opposition.

The insights of this early work are still being taught in recently published meteorological textbooks, e.g. Harrison [4]. In [4], Harrison clearly explains the basic physics of the interaction of a temperature sensor with flowing air and arrives at the prediction that the radiative error of a thermometer depends on the square root of the diameter of the sensor and inversely on the square root of the air speed past the sensor.

However these results are only hinted at in the 2014 edition of the definitive guide for meteorological measurements produced by the Commission on Instruments and Methods of Observation (CIMO) of the World Meteorological Organisation (WMO) [19].

The CIMO Guide notes that, when directly exposed to the Sun, 'For some thermometer elements, such as the very fine wire used in an open-wire resistance thermometer, the difference (from true air temperature) may be very small or even negligible. However, with the more usual operational thermometers the temperature difference may reach 25 K under extremely unfavourable conditions. Therefore, in order to ensure that the thermometer is at true air temperature it is necessary to protect the thermometer from radiation by a screen or shield that also serves to support the thermometer...'.

They then use an operational definition of air temperature as 'the temperature indicated by a thermometer exposed to the air in a place sheltered from direct solar radiation', but simultaneously acknowledge that the design of thermometer screens has an effect on the measured temperature. They state that 'the temperature of the air in a screen can be expected to be higher than the true air temperature on a day of strong sunshine and calm wind, and slightly lower on a clear, calm *night, with errors perhaps reaching 2.5 K and −0.5 K, respec*tively, in extreme cases'. They note that 'Screens with forced ventilation, in which air is drawn over the thermometer element by a fan, may help to avoid biases when the microclimate inside the screen deviates from the surrounding air mass. Such a deviation only occurs when the natural wind speed is very $low (< lm s^{-1})$ ', i.e. there is no mention of the radiative error within screens, only that the air itself is warmer within the screen.

Radiative error is just one of several systematic 'thermometer exposure' effects, and there is value—particularly for climate studies—in the simple propagation of past practices, even when they are known to be subject to systematic effects. It is the consistency of measurement practices over decades that allows the unambiguous extraction of climate trends. So there is considerable merit to a conservative approach to new meteorological technology. Both climatologists and meteorologists are keen to avoid having to compensate for a change in exposure, even if the new answers are closer to 'the correct' answer. Nonetheless, meteorological technology has advanced and will advance in the future and it is likely that good designs which reduce errors at modest expense will eventually be adopted, especially in any new stations designed for use as climate reference stations.

The effect of radiative errors within thermometer screens is calculated by Erell, Leal and Maldonado [20] and they arrive at conclusions similar to Harrison [4]: i.e. that the radiative error depends on the square root of the diameter of the sensor and inversely on the square root of the air speed past the sensor.

In [21, 22], Harrison *et al* describe the design and testing of fine-wire platinum resistance thermometers (PRTs), which have a relatively small radiative correction. Harrison then uses these sensors to assess errors in a standard Stevenson Screen [23].

Bugbee [24], in a presentation at *Meteorological World* in Brussels in November 2015, discussed the problems of air temperature measurement and concluded that for air temperature measurements, 'small is best'. Figure 1 shows data [25] demonstrating that when subject to large irradiance, smaller

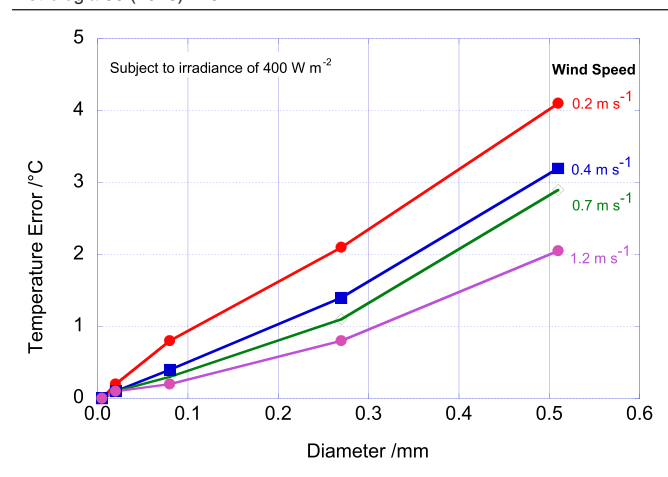


Figure 1. Data from Bugbee [25] showing the dependence of the radiative temperature error on 'wire diameter' for thermocouple sensors exposed to 400 W m^{-2} at various wind speeds.

diameter sensors give better results—closer to true air temperature—than larger ones.

1.4. Summary

The purpose of these short reviews of the metrological and meteorological literature has been to show that although the dependence of radiative errors on sensor diameter and air speed has been reported previously, there is also a surprising absence of reporting on the effect in places where it might reasonably have been expected.

2. Heat transfer model

2.1. Model details

In this section we describe a model of the relatively simple case of air flowing perpendicularly over a long cylinder (figure 2). Our purpose in creating this model is not to create a comprehensive theory, which is beyond the scope of this work, rather our intention is to highlight the key physical mechanisms underlying the 'sensor size' effect. We can imagine our model cylinder to represent either a temperature sensor or a cylindrical object whose steady-state temperature is determined by the balance of internal heating, radiative exchange with the environment and heat transfer with the flowing air.

In our simple model we consider air at temperature T_A flowing at speed V past a cylindrical object of length L, diameter D, surface area A and surface temperature T_S . We consider only the case when $L \gg D$. There are four ways in which heat may be exchanged with the cylinder.

Firstly, heat may be dissipated inside the cylinder, for example by the electrical current passing through a sensor. Secondly, the cylinder may absorb 'direct' radiation—normally in the optical region of the spectrum—such as sunlight or room lighting. Thirdly, it may receive radiant energy—typically in the infrared region of the spectrum with wavelengths $\sim 10~\mu m$ —from the walls of the room or the environment. For simplicity this is assumed to be characteristic of a blackbody with temperature $T_{\rm W}$.

The cylinder also radiates energy at similar wavelengths, and we assume the spectrum of this radiation to be characteristic of a grey body with emissivity ϵ_S , and temperature T_S . We note that use of a single emissivity is a simplification, since ϵ_S is likely to be wavelength-dependent, having different values for long wavelength thermal radiation and short-wavelength optical illumination.

Finally, the cylinder can exchange heat with the flowing gas with which it is in direct contact.

We want to find out how the steady-state value of $T_{\rm S}$ varies with air speed and cylinder diameter for a situation under combined thermal and direct irradiation. If the cylinder is a temperature sensor, then $T_{\rm S}$ is likely to be a good estimate for the temperature, which will be inferred when the sensor is read. If the cylinder is a hollow object, then $T_{\rm S}$ is likely to be a good estimate for the temperature, which will be reported by a temperature sensor placed within the object.

2.2. Self-heating and direct irradiance

We assume that direct heating of the cylinder can arise from self-heating within the cylinder and from direct irradiation. The rate of self-heating, \dot{Q}_{SH} , will be given by:

$$\dot{Q}_{\rm SH} = I^2 R. \tag{1}$$

For a Pt100 sensor at 20 °C the resistance R is approximately 108 Ω and for a current of I=1 mA, \dot{Q}_{SH} amounts to approximately 0.1 mW.

Direct irradiation may or may not have a blackbody spectrum and so we simply specify the irradiance E in watts per square metre, rather than an equivalent blackbody temperature and solid angle.

For an opaque cylinder of length L and diameter D with emissivity (= absorptivity) $\epsilon_{\rm S}$ illuminated perpendicular to an irradiant beam, the rate at which energy is absorbed is:

$$\dot{Q}_{\text{Direct}} = \epsilon_{\text{S}} LDE. \tag{2}$$

In this expression we have assumed that the angular emissivity can be approximated by the total hemispherical emissivity $\epsilon_{\rm S}$, something which is unlikely to be true for most surfaces. A more accurate expression would include a factor—probably between 0.5 and 1—to account for lower emissivity at lower angles of incidence. However, in the context of this work neither the total hemispherical emissivity nor the angular dependence of emissivity are well known. So in this context we will omit this 'angular factor' and consider the concomitant error to be included in the—generally large—uncertainty associated with $\epsilon_{\rm S}$.

2.3. Thermal radiation from the environment

When considering the emission and absorption of thermal radiation—typically with a peak intensity at a wavelength of the order of $10 \, \mu m$ —we assume that the sensor surface has the same emissivity (and absorptivity) ϵ_S as in the optical region of the spectrum. This is unlikely. So, in addition to the caveats concerning the angular dependence of ϵ_S , we also record

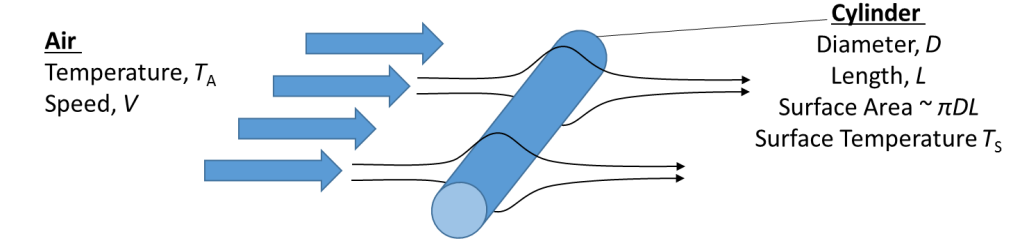


Figure 2. A cross-sectional view of the general arrangement under consideration.

similar caveats concerning the wavelength dependence of ϵ_s . If in our experimental work we were able to clearly separate thermal and direct radiation, it might become necessary to use a wavelength-dependent emissivity. For this work we consider ϵ_s to represent an effective emissivity.

If the walls surrounding the sensor radiate as a blackbody at temperature $T_{\rm W}$, then the rate at which radiant power is absorbed by the sensor is:

$$\dot{Q}_{\text{Radiant-in}} = \epsilon_{\text{S}} \sigma A T_{\text{W}}^4 \tag{3}$$

where σ is the Stefan–Boltzmann constant. The power radiated by the sensor is:

$$\dot{Q}_{\text{Radiant-out}} = \epsilon_{\text{S}} \sigma A T_{\text{S}}^4. \tag{4}$$

Thus the net power received from the walls can be written as:

$$\dot{Q}_{\text{Radiant-net}} = \epsilon_{\text{S}} \sigma A \left(T_{\text{W}}^4 - T_{\text{S}}^4 \right). \tag{5}$$

For small differences between $T_{\rm W}$ and $T_{\rm S}$, equation (5) may be simplified to:

$$\dot{Q}_{\text{Radiant-net}} \approx 4\sigma\epsilon_{\text{S}}AT_{\text{W}}^3 \left(T_{\text{W}} - T_{\text{S}}\right)$$
 (6)

where the error is of order $\frac{3}{2}\frac{\Delta T}{T_{\rm W}}$, which is less than 1% for the situations envisaged in the laboratory and wall temperatures within 2 °C of the air temperature. Even in the more extreme situations which might be encountered in meteorological exposures, $\dot{Q}_{\rm Radiant-net}$ will still vary *approximately* linearly with $(T_{\rm W}-T_{\rm S})$, and in absolute magnitude, the uncertainty in the emissivity of the sensor surface is likely to be considerably more significant.

We note that heating from direct irradiation (equation (2)) depends on the cross-sectional area of the sensor exposed to the irradiance, whereas the relevant area for thermal irradiation (equation (6)) is the entire surface area of the sensor. However, both areas scale linearly with the sensor diameter.

2.4. Heat transfer coefficient

The basic equation describing heat exchange with the air is:

$$\dot{Q}_{\text{Flow}} = hA \left(T_{\text{S}} - T_{\text{A}} \right) \tag{7}$$

where h is the heat transfer coefficient. For air flowing perpendicularly past a cylinder at speed V, h is given by equation (7.35) of Çengal and Ghajar [14] as:

$$h = \frac{k}{D} \operatorname{Nu}_{\text{Cyl}} \tag{8}$$

where k is the thermal conductivity of the air and Nu_{Cyl} is the Nusselt number for a cylinder in a transverse air flow. Nu_{Cyl} is approximately the ratio of heat transport by convection to heat transport through static gas, and depends in a complex way on the interaction of the air flow with the cylinder. Several expressions are commonly used to parameterise Nu_{Cyl} [14], but for a wide range of air speeds and diameters the expression below can be used with an uncertainty of approximately 30%:

$$Nu_{Cyl} = 0.3 + \frac{0.62Re^{\frac{1}{2}} \Pr^{\frac{1}{3}}}{\left[1 + \left(\frac{0.4}{Pr}\right)^{\frac{2}{3}}\right]^{\frac{1}{4}}} \left[1 + \left(\frac{Re}{282\,000}\right)^{\frac{5}{8}}\right]^{\frac{4}{5}}$$
(9)

where Re is the Reynolds number describing the flow and Pr is the Prandtl number describing the air. The Reynolds number is given by:

$$Re = \frac{VD}{\nu} = \frac{\rho VD}{\mu} \tag{10}$$

where ν is the kinematic viscosity of air, ρ is the air density and μ is the air viscosity; the air velocity is V and the cylinder diameter is D. The Prandtl number is given by:

$$\Pr = \frac{\nu}{\alpha} = \frac{\mu c_p}{k} \tag{11}$$

where α is the air thermal diffusivity and c_p is the specific heat capacity of the air.

Çengal and Ghajar [14] state that the expression summarised in equation (10) is valid when Re·Pr > 0.2, which for a 0.5 mm diameter cylinder in air at 20 °C corresponds to a minimum air speed of ~0.01 m s⁻¹. The upper limit is for Reynolds numbers ~4 × 10^5 , which corresponds to fast moving air. For sensors with a diameter of 6 mm, air speeds in the range 1 m s⁻¹ to 10 m s⁻¹ correspond to Reynolds numbers between 400 and 4000. If required, the 30% uncertainty in equation (9) could be reduced for a limited range of air speeds and sensor diameters.

2.5. Steady-state solution

We now have two rate relationships that determine the surface temperature of a cylindrical object or sensor immersed in flowing air. In the steady state, the heat flux into the air (equation (7)) must balance the fluxes due to irradiation (equations (2) and (6)) and the self-heating (equation (1)), i.e.

$$hA\left(T_{S}-T_{A}\right)=\left[I^{2}R+\epsilon_{S}LDE\right]+4\sigma\epsilon_{S}AT_{W}^{3}\left(T_{W}-T_{S}\right). \tag{12}$$

Solving for T_S we find:

$$T_{\rm S} = \frac{\left[I^2R + \epsilon_{\rm S}LDE\right] + 4\sigma\epsilon_{\rm S}AT_{\rm W}^4 + hAT_{\rm A}}{\left(hA + 4\sigma\epsilon_{\rm S}AT_{\rm W}^3\right)}.$$
 (13)

If we assume that the radiative environment is at the same temperature as the cylinder surface (i.e. $T_{\rm W}=T_{\rm S}$), and consider only internal heating and direct irradiation, then this expression simplifies to:

$$(T_{\rm S} - T_{\rm A}) = \frac{\dot{Q}_{\rm Flow}}{hA} = \frac{\dot{Q}_{\rm Flow}D}{kA\,{\rm Nu}_{\rm Cyl}}.$$
 (14)

For air at atmospheric pressure and at typical laboratory temperatures, we can simplify expressions 9 to 11 for Nu_{Cyl} to extract a simplified dependence on air speed and probe diameter. At low air speeds it is reasonable to expect that the temperature error $(T_S - T_A)$ will scale roughly as:

$$(T_{\rm S} - T_{\rm A}) \propto \dot{Q}_{\rm Flow} \left(\frac{D}{V}\right)^{\frac{1}{2}}$$
 (15)

i.e. we would expect a square root dependence on cylinder diameter and an inverse square root dependence on flow speed. This is in agreement with the conclusions in [3, 4, 13, 14, 16, 20, 23].

The inverse square-root dependence on flow speed (equation (15)) does not extend to static air because of the lower Reynolds number limit of applicability of equation (9). However, it does extend to air which would, for most practical purposes, would be considered static. For a 0.1 mm diameter cylinder in air at 20 °C, the lower limit of applicability is approximately 0.005 m s⁻¹. For larger diameter probes, the lower air speed limit is proportionately lower.

2.6. Evaluation of the model for a laboratory environment

2.6.1. Specifications. In order to give an insight into the magnitudes of the quantities involved in equation (13), figures 3–7 describe the steady-state radiant heating of cylinders which might be plausibly encountered in laboratory situations. We consider a wide range of cylinder diameters even though temperature sensors are generally only a few millimetres in diameter. The smaller diameters are included to show that even for sensors with the smallest diameters, errors may still be significant. The larger diameters—up to 1 m—are included to show that in the limit of large objects, cooling (or heating) by flowing air is ineffective.

The results are generally only weakly dependent on sensor length, but these specific calculations have been carried out assuming a length of 15 mm. We assume no direct irradiation, $E=0~\rm W~m^{-2}$, i.e. a dark room with air at $T_{\rm Air}=20~\rm ^{\circ}C$ and walls one degree warmer: $T_{\rm Wall}=21~\rm ^{\circ}C$. The sensor surface is considered to be black ($\epsilon_{\rm S}=1$) except for section 3.6.4, where the effect of sensor emissivity is investigated. Under these conditions, the radiation incident upon a 3 mm diameter sensor 15 mm long is approximately 1.07 mW, which is about ten times larger than the self-heating in a Pt100 sensor with a current of 1 mA and resistance of 108 Ω .

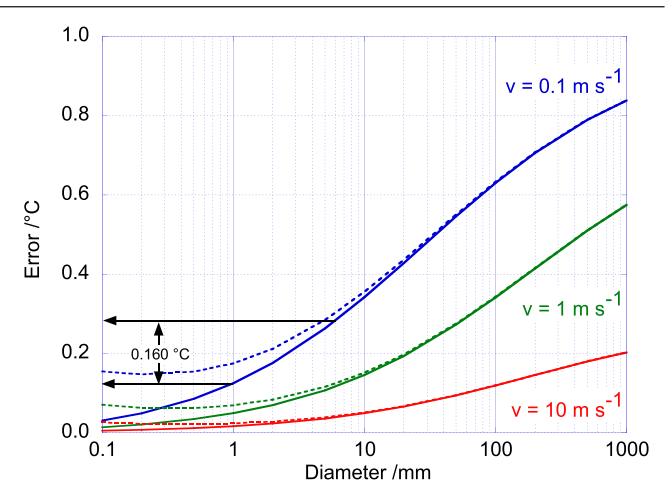


Figure 3. Dependence of the calculated radiative heating on cylinder diameter. Results are shown for air speeds of $0.1~{\rm m~s^{-1}}$, $1~{\rm m~s^{-1}}$, and $10~{\rm m~s^{-1}}$. The dashed curves—which include the effect of sensor self-heating—do not tend to zero error at small diameters. Notice that larger objects are weakly cooled by the air. Also shown is the $0.160~{\rm ^{\circ}C}$ predicted difference between two calibrated 'black' sensors with diameters of 1 mm and 6 mm after correction for selfheating.

2.6.2. Variation with cylinder diameter. Figure 3 shows the dependence of the calculated radiative heating on cylinder diameter for air speeds of 0.1 m s⁻¹, 1 m s⁻¹ and 10 m s⁻¹. These curves are shown as solid lines, and curves with dotted lines show the effect of intrinsic self-heating. As expected, higher flow speeds yield lower temperature errors.

However the most interesting feature of figure 3 is the variation in radiative heating with sensor size. For example, two calibrated sensors which differ only in their diameter (1.0 mm and 6.0 mm) will yield readings which differ by approximately 0.16 °C. This would be true even if the sensors were thermocouples with no internal power dissipation. Additionally, at an air speed of 0.1 m s⁻¹, both sensors would indicate a result more than 0.1 °C warmer than the true air temperature.

Figure 4 shows the effect of sensor size with no irradiation, either direct or blackbody, but only intrinsic self-heating due to dissipation of approximately 0.1 mW in the sensor. Now the increased sensor size *reduces* the self-heating correction by lowering the heat flux density at the sensor surface. In the $V = 0 \,\mathrm{m \, s^{-1}}$ (static air) limit [16] the heating for a sensor 15 mm long with $D = 0.1 \,\mathrm{mm}$ would be approximately 0.25 °C, and approximately 0.1 °C for a sensor with $D = 3 \,\mathrm{mm}$; i.e. slightly greater than the calculated heating for $V = 0.1 \,\mathrm{m \, s^{-1}}$.

We show this figure simply to stress that the self-heating component of sensor heating can be estimated by increasing the measurement current by a factor $\sqrt{2}$ (which doubles the heating) and then extrapolating to an estimated zero-current temperature [5]. In contrast, however, there is no obvious way to estimate the radiative loading, or indeed to even detect if there is any radiative heating, and hence infer the 'true' air temperature.

2.6.3. Variation with air speed. Figure 5 shows the dependence of the calculated radiative heating on air speed for a selection of cylinder diameters. It shows that at low air speeds,

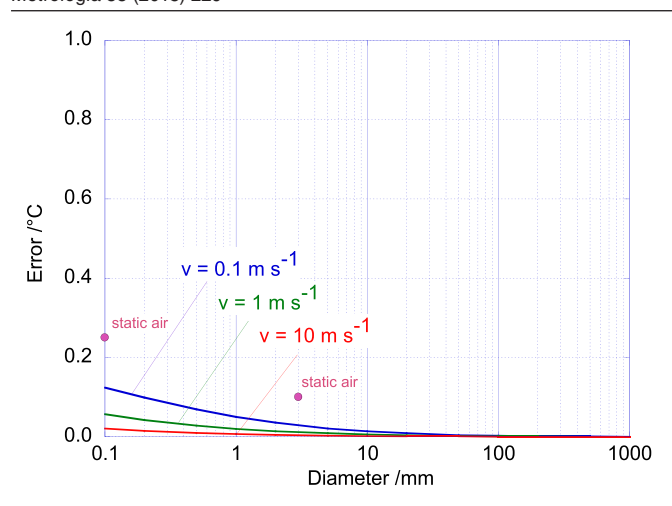


Figure 4. The dependence of the calculated self-heating on the cylinder diameter. Results are shown for air speeds of 0.1 m s^{-1} , 1 m s^{-1} , and 10 m s^{-1} . Two additional points are shown for static air. This graph shows that smaller resistive sensors show a larger self-heating effect due the increased heat flux density at the sensor surface.

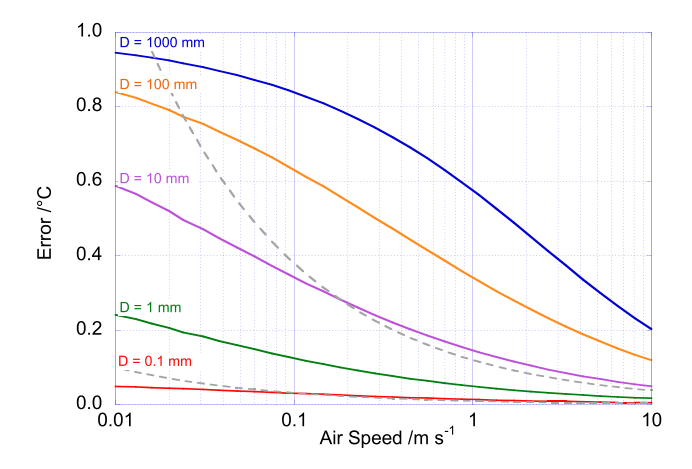


Figure 5. Dependence of the calculated radiative heating on air speed. Results are shown for diameters 0.1 mm, 1 mm, 10 mm, 100 mm and 1000 mm. In this situation, the dashed grey curves show that an inverse square root dependence does not accurately describe the air speed dependence. See text for details.

a radiative environment just 1 °C warmer than the sensor can result in errors of several tenths of a degree for plausibly sized sensors. Additionally, the figure shows that in a laboratory, large objects will simply not be cooled by the air flow for any plausible air speed. Thus a 100 mm diameter object placed in the laboratory may differ in temperature significantly from a 6 mm diameter thermometer placed in the air next to it.

The expected inverse square root dependence of the temperature error with air speed (equation (15)) is not observed here, because the effective radiative load varies with the difference between the temperature of the cylinder surface and the environment.

2.6.4. Variation with emissivity. Figures 6 and 7 show the heating of the cylinders for different surface emissivities. Figure 6 shows the effect of emissivity at an air speed of 0.1 m s⁻¹, so the $\epsilon = 1$ curve corresponds to the top-most curve in figure 3.

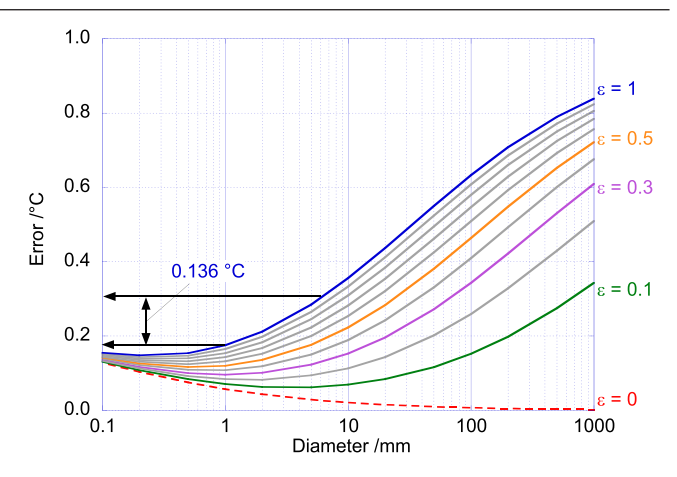


Figure 6. The dependence of the calculated radiative heating on cylinder diameter. The results are shown for surface emissivities from 0 to 1. The environment is as described in section 3.6.1 with an air speed of 0.1 m s^{-1} . Notice that large objects are barely cooled by the air but that sensor self-heating is more important for small objects. Also shown is the 0.136 °C predicted difference between two calibrated 'black' sensors with diameters of 1 mm and 6 mm. Notice that the curves do not reach zero due to sensor self-heating.

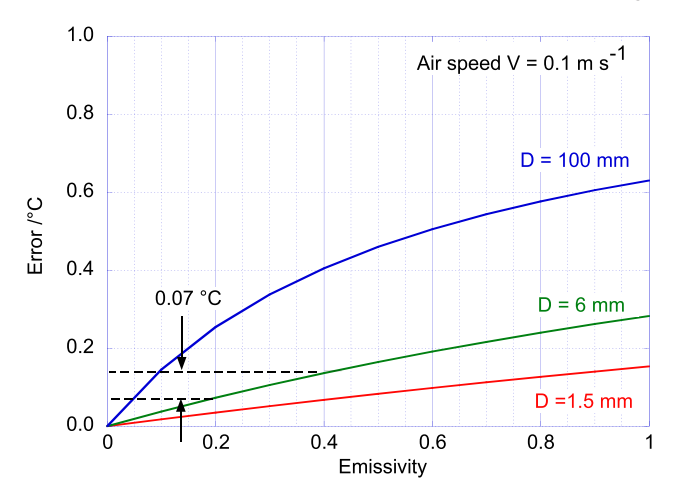


Figure 7. Dependence of the calculated radiative heating on emissivity. Results are shown for three different sensor diameters in an air flow of $0.1~{\rm m~s^{-1}}$. Notice that for an emissivity of 0.3, an uncertainty of ± 0.1 in the emissivity of a 6 mm diameter sensor sheathed in stainless steel gives rise to an uncertainty in the radiative correction of $\pm 0.035~{\rm °C}$ —about 30% of the total radiative error

Unsurprisingly, reducing the emissivity of the sensor surface (i.e. making it shinier) significantly reduces the radiative heating. The effect is approximately linear for small cylinder diameters typical of temperature sensors, but non-linear for larger objects for which the surface temperature approaches the wall temperature. This non-linearity is shown more clearly in figure 7.

One conclusion which can be drawn from the results presented in figure 7 is that it is difficult to assess the extent of radiant errors from first principles. For example, the emissivity of stainless steel, which is commonly used to enclose sensors, can take a wide range of values between roughly 0.1 and 0.8, depending on its composition and the extent to which it is polished. Even assuming a modest variation of $\epsilon = 0.3 \pm 0.1$ in this hypothetical laboratory environment, a calibrated 6 mm

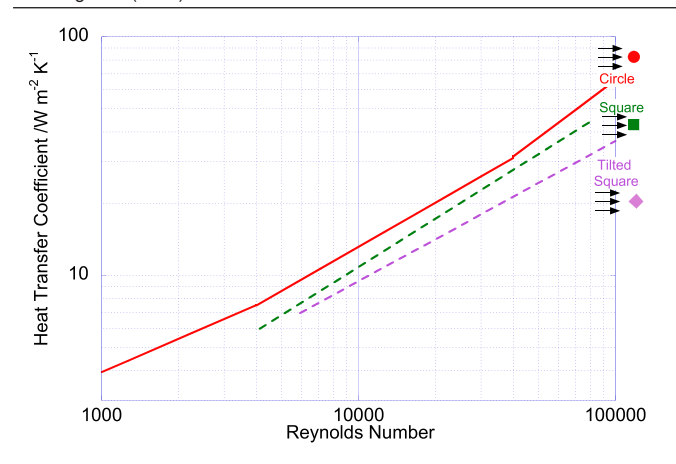


Figure 8. Heat transfer coefficient for air flowing past (a) a cylinder of diameter D (red line) or (b) a shape with a square cross-section with a side of length D and facing the air stream flat (green dotted line) or (c) a shape with a square cross-section with side of length D facing the air stream at an angle (purple dotted line). The Reynolds number of 10 000 corresponds to an air speed of approximately $1.5 \, \mathrm{m \, s^{-1}}$ around an object with a characteristic size $D = 10 \, \mathrm{cm}$.

diameter sensor sheathed in stainless steel could give values varying by ± 0.035 °C.

2.6.5. Variation with cross-section. The results in figures 3–7 are broadly insensitive to the cross-sectional shape facing the airstream. Figure 8 shows the heat transfer coefficient of a cylinder of diameter D and a shape with a square cross-section and a side of length D, facing the air stream either flat or at an angle. The Reynolds number of 10 000 corresponds to an air speed of approximately 1.5 m s⁻¹ around an object with a characteristic size D = 10 cm [13, 14].

2.6.6. Spheres. Bare glass-encapsulated thermistor sensors may be more reasonably modelled as small spheres rather than cylinders. For spheres, the theory leading up to equation (13) is repeated but with the following changes. Firstly, the sensor surface area and cross-sectional area are modified to those relevant to a sphere, and secondly the heat transfer coefficient Nu_{Sph} appropriate to a sphere (see equations (7)–(36) in [14]) is used instead of Nu_{Cyl} (equation (9)):

$$Nu_{Sph} = 2 + \left[0.4Re^{\frac{1}{2}} + 0.06Pr^{\frac{2}{3}} \right] Pr^{0.4} \left(\frac{\mu_{Stream}}{\mu_{Surface}} \right)^{\frac{1}{4}}.$$
 (16)

In equation (16), μ is the viscosity of the air, the subscript 'Stream' indicates evaluation far away from the sphere and the subscript 'Surface' indicates evaluation at the surface of the sphere. The expression is valid for $3.5 \le \text{Re} \le 8 \times 10^4$, $0.7 \le \text{Pr} \le 380$ and $1.0 \le (\mu_{\text{Stream}}/\mu_{\text{Surface}}) \le 3.2$.

Figure 9 shows the ratio of the calculated temperature errors for a sphere 3 mm in diameter and a cylinder of the same diameter, 15 mm in length. When self-heating is negligible (solid curves) the temperature error of a spherical sensor is less than the cylinder at all air speeds, with a very significant improvement at low air speeds. When equal amounts of self-heating (0.1 mW) are considered, the spherical sensor exhibits a larger error than the cylindrical sensor at high flow speeds. However, because of the size dependence of the heat transfer function, at

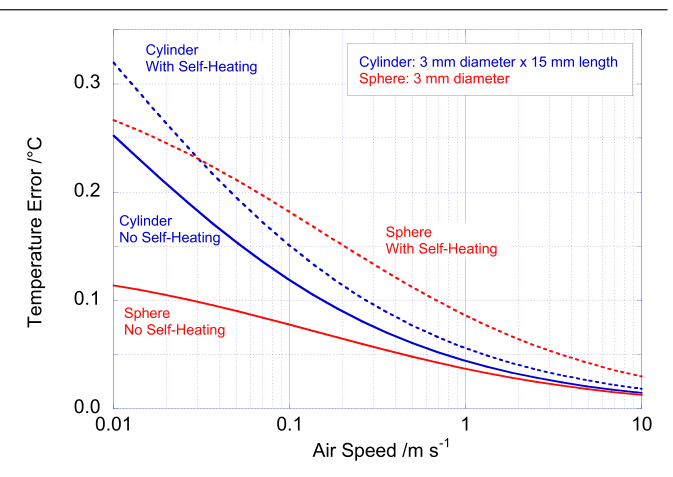


Figure 9. The predicted temperature error versus air speed for spherical and cylindrical sensors 3 mm in diameter. The cylindrical sensor is assumed to be 15 mm long. The solid lines show the case for no internal power dissipation, and the dashed lines show the case where the two sensors experience the same dissipation (\sim 0.1 mW). See text for details.

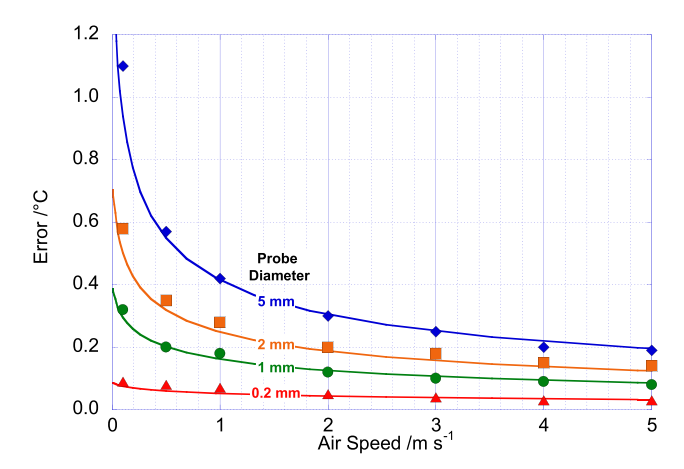


Figure 10. Dependence of the calculated magnitude of radiative cooling on air speed for sensors subject to a radiant environment at 5 °C when the air temperature is 15 °C. The results are shown for four different sensor diameters. The solid lines show an evaluation of equation (13) modified for a sphere as described in section 3.6.6. The individual data points are those calculated by Erell *et al* [19]. See the text for discussion.

the lowest flow speeds, the spherical sensor again has a lower error. We note that in some ways the comparison in figure 9 is not fair because the resistance and sensitivity of a (spherical) thermistor are generally much larger than for a (cylindrical) PRT. Thus thermistors can often be operated with a much lower power dissipation than a PRT. Additionally, we note that sensor self-heating can always be detected and corrected by changing the measuring current, whereas there is no simple way to identify when a sensor is subject to a radiative error.

2.7. Comparison with previous work

Figure 10 shows a comparison with Erell *et al*'s calculations for spherical sensors subject to a radiative environment at 5 °C when the air temperature is 15 °C, but with no direct irradiation (figure 3 of [20]). For an assumed emissivity of 0.5, there is good agreement with Erell *et al*.

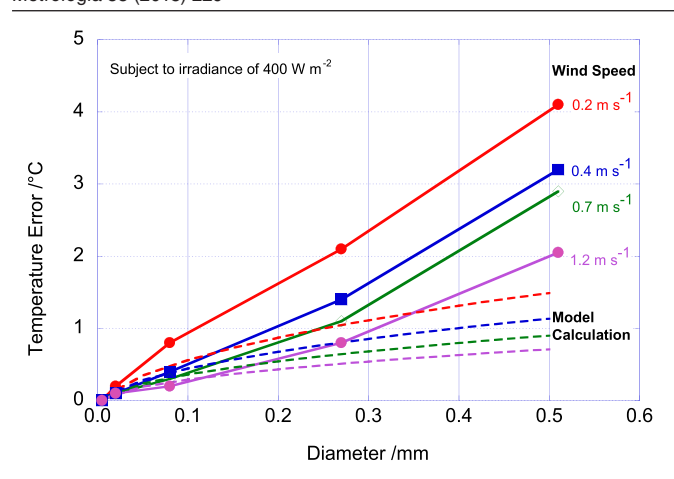


Figure 11. Model calculations (dotted lines) for the situation described by Bugbee [21] and comparison with Bugbee's data, also shown in figure 1. See text for discussion.

Harrison's fine-wire thermometer [21–23] was made of 500 mm of 0.025 mm diameter platinum wire held over a frame, and excited with a measurement current of 50 μ A. He states that experimentally the warming due to irradiance is less than 70 mK per 100 W m⁻² for wind speeds greater than 1 m s⁻¹ measured at a height of 2 m. Evaluating equation (13) for similar circumstances predicts a temperature rise of only ~20 mK per 100 W m⁻² for an air speed of 1 m s⁻¹ assuming an emissivity of 0.5 for the platinum wire.

Unfortunately Harrison's wind speed specification does not refer to the air speed at the sensor, but instead to that measured at a height of 2 m: the air speed at the sensor is likely to be slightly lower and the warming greater. Neither is the air speed guaranteed to be perpendicular to the axis of the wire as we assume in our calculations. These factors could account for some, but probably not all of the difference between Harrison's data and these calculations.

Finally, we can also plot the modelled curves (figure 11) for a situation relevant to the data reported by Bugbee [25] and reproduced in figure 1. It is clear that the modelled data cannot account for all the heating reported by Bugbee, even assuming an emissivity of 1. Additionally, the square root dependence predicted by the theory is absent from the data. Bugbee reports the 'diameter' as 'the diameter of the thermocouple wire', so it could be that the physical cross section of the sensor is larger than indicated by the wire due to insulation and sheathing. However, we have no explanation for why the square root dependence is not observed.

Overall we conclude that equation (13) gives a plausible agreement within a factor of approximately two of the previous calculations and measurements. However meteorological exposures are complex and ideally we would test equation (13) in a wider variety of well-characterised exposures.

3. Measurements

3.1. Apparatus

To assess the effects predicted by equation (13), experiments were conducted in two laboratories at NPL which are used

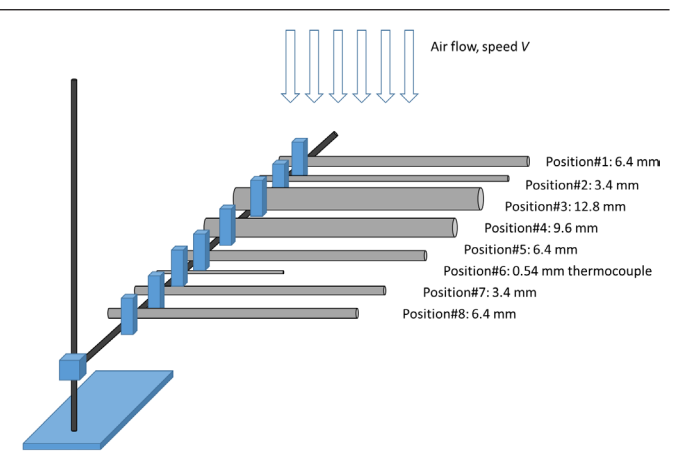


Figure 12. Apparatus used to detect radiative errors consists of seven stainless steel tubes of four diameters, approximately 30 cm in length held at one end in a clamp stand. The laboratory air flows vertically downward across the tubes. Three 6.4 mm diameter tubes are used as controls to check for systematic changes in air temperature from one end of the apparatus to the other. Also, in position #6 is a 0.54 mm diameter type MIMS thermocouple (TC1 in figures 13 and 17). During operation, a probe thermocouple is moved from one tube to the next to investigate differences in temperature.

for dimensional measurements, and in which the temperature and air flow are exceptionally closely controlled. Although the temperature cannot be varied (as in a climatic chamber), the combination of excellent temperature stability ($\sim \pm 0.01~^{\circ}\text{C})$ combined with low, steady, unidirectional air flow is uniquely well-suited to these tests.

The apparatus consists of a series of stainless steel tubes held at one end in a clamp stand and exposed horizontally to the vertical air flow in the laboratory (figure 12).

Seven stainless steel tubes with external diameters 12.8 mm, 9.6 mm, 6.4 mm, 3.4 mm were used. The surface finish of the tubes was visually similar. The temperatures of the 9.6 mm and 12.8 mm tubes were monitored by inserting type-K thermocouples, and their average was used as a 'reference' temperature to compensate for small variations in laboratory temperature. Additionally, a 0.54 mm diameter rapidly-responding mineral-insulated metal-sheathed (MIMS) type-K thermocouple was exposed alongside the tubes.

To avoid a systematic bias with the position arising from an air temperature gradient in the laboratory, the tubes were not positioned in size-order on the clamp stand, and two extra 6.4 mm diameter tubes and one extra 3.4 mm diameter were used to check for any variation with position.

Before embarking on this work, it would have previously been the strong expectation of the authors that after allowing time for equilibration, all these tubes would 'obviously' acquire the temperature of the air flowing past them. In fact this is not the case and in the steady state the temperature of each tube is different.

The temperature differences between the tubes were monitored by moving a 0.25 mm 'probe' type-K MIMS thermocouple from one tube to the next. By moving a single thermocouple, (rather than comparing the results from multiple thermocouples) no shifts in calibration need be accounted for. In this application, thermocouples are the sensor of choice

because they are available in narrow diameters and have no internal self-heating which might obfuscate the radiative heating effect. A *National Instruments* NI9211 thermocouple logger (using an internal cold-junction compensation scheme) monitored the temperature of all four thermocouples once per second

The probe thermocouple was checked by immersing it in an oil-bath kept at $20.0\,^{\circ}\text{C}$ with a small correction ($-0.141\,^{\circ}\text{C}$) applied. When exposed together in a small copper enclosure shielded from air flows, the other three thermocouples agreed with the probe thermocouple within $\pm 0.12\,^{\circ}\text{C}$ and small corrections ($0.015\,^{\circ}\text{C}$, $0.095\,^{\circ}\text{C}$ and $0.115\,^{\circ}\text{C}$) were applied to make the thermocouple readings self-consistent within approximately $0.01\,^{\circ}\text{C}$. However, we emphasise that none of the key results rest on the calibration of the thermocouples. We rely only on the stability of the cold-junction compensation—which can be judged by the stability of the unchanging channels (TC3 and TC4 in figures 14 and 17)—and the linearity and adherence to the nominal sensitivity of a single thermocouple in the range between 19 $^{\circ}\text{C}$ and 20 $^{\circ}\text{C}$.

3.2. Laboratory environments

The circumstances of this work limited our ability to carry out an assessment of the air flow and radiant environment of the laboratories with the metrological rigour we would normally choose. Instead, all that was possible were indicative measurements of the laboratory environment. However we stress that the conclusion of the diameter-dependence of the radiant heating is not affected by this inexactitude.

The low-speed steady air flow in the two laboratories was measured using a 'hot probe' anemometer and estimated to be 0.11 m s $^{-1}$ with intermittent fluctuations in the range ± 0.04 m s $^{-1}$ in the region of the tubes in both laboratories.

The radiative environment is difficult to assess exhaustively, but an indicative measurement was made by recording the temperature with a non-contact infrared thermometer (viewing ratio 1:8) placed at the location of the tubes and pointing in six directions (up, down, left, right, front, back). In laboratory 1 the readings were: 20.4 °C, 20.4 °C, 20.4 °C, 20.4 °C, 20.4 °C, 20.4 °C and 20.4 °C; in laboratory 2 the readings were: 20.0 °C, 20.2 °C, 20.4 °C, 20.2 °C, 20.4 °C and 20.4 °C. The thermometer was then pointed at close range into an oil bath at 20.0 °C and was seen to read 20.8 °C. Applying a -0.8 °C correction, we thus estimate the indicative radiative temperature in laboratory 1 to be 19.5 °C and in laboratory 2 to be 19.6 °C.

In both laboratories, lighting fixtures are placed high on the walls where light from LED sources is reflected into the laboratories from white panels through a transparent plastic window. The temperature in the region of these lighting panels was locally ~2 °C warmer than the general laboratory temperature, but the panels subtend a small solid angle from the location of the sensors ($\sim 4\pi/20$ steradians).

Within laboratory 1 the visible light level in the lab was recorded to be approximately 1180 lumens m^{-2} from the ceiling and 160 lumens m^{-2} from the floor and in laboratory

Table 1. Summary of the key environmental parameters in laboratories 1 and 2. All the estimates should be taken as indicative only.

	Wall (°C)	Air (°C)	Direct irradiance (W m ⁻²)
Laboratory 1	19.5	19.3	10.6
Laboratory 2	19.6	19.7	8.2

2, the readings were 890 lumens m^{-2} from the ceiling and 150 lumens m^{-2} from the floor. Adding these illuminances together yields 1340 lumens m^{-2} in laboratory 1, and 1040 lumens m^{-2} in laboratory 2. Without detailed spectral measurements we cannot convert these illuminances into irradiance estimates, but if the illumination were similar to a solar spectrum, then we would expect conversion factors between ~0.007 and ~0.01. We chose to use a figure of 0.0079 W lumen⁻¹, which would correspond to irradiances of 10.6 W m^{-2} and 8.2 W m^{-2} respectively. We stress again that these figures should be viewed as purely indicative because we cannot readily assess their uncertainty, which is likely to be large.

Unfortunately, due to the requirement of keeping the laboratory temperature stable—the laboratories are used routinely for calibrations—it was not possible to simply switch off the lights. However, we note that our estimate of the irradiation from the lights was larger than our estimate of irradiation from the environment.

To illustrate the relative significance of the various environmental influences summarised in table 1, we consider a 20 mm long Pt100 probe with a 3 mm diameter stainless steel case and an emissivity of 0.5. If the environment is 0.1 °C warmer than the air, there is an irradiance of 10 W m $^{-2}$ and a measuring current of 1 mA, then the thermal loads on the sensor are 0.27 mW due to thermal irradiation, 0.75 mW due to illumination and 0.11 mW due to self-heating.

3.3. Measurement procedure

In each laboratory, the tubes were left to stabilise, and after stabilisation the temperatures were stable to within $\pm 0.01~^{\circ}\mathrm{C}$ over several hours. Once stabilised, the experimenter entered the room, moved the probe thermocouple from one tube to the next, and then left the room. Typically there would be a transient temperature change in the probe thermocouple and also the thin MIMS thermocouple exposed alongside the tubes. The experimenter would then leave the room for a few minutes. Overall it took approximately 40 min to move the thermocouple and read the temperatures within each tube.

In a normal laboratory, air temperature variations over 40 min would be likely to create temperature drifts amongst the tubes in which any systematic variation of temperature with tube diameter might easily be obscured. It is the exceptional temperature stability and uniformity within these laboratories that makes this experiment possible.

In figures 13, 14, 16 and 17, the 10 s running average of the thermocouple reading is plotted.

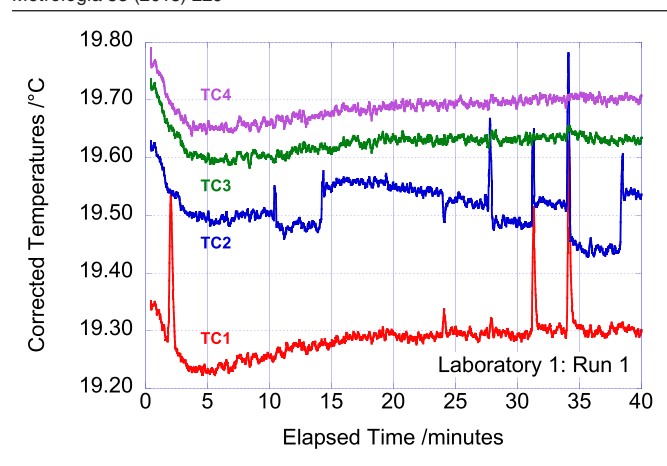


Figure 13. Data from laboratory 1 showing a 10 s running average of thermocouple readings corrected to be approximately self-consistent as described in the text. TC1 is the reading from a 0.54 mm diameter thermocouple exposed alongside the tubes. TC2 is the probe thermocouple which is moved from tube to tube. TC3 and TC4 are in the 9.6 mm and 12.8 mm diameter tubes and are used to create a reference temperature which tracks slow changes in air temperature—visible here in the first few minutes of the data.

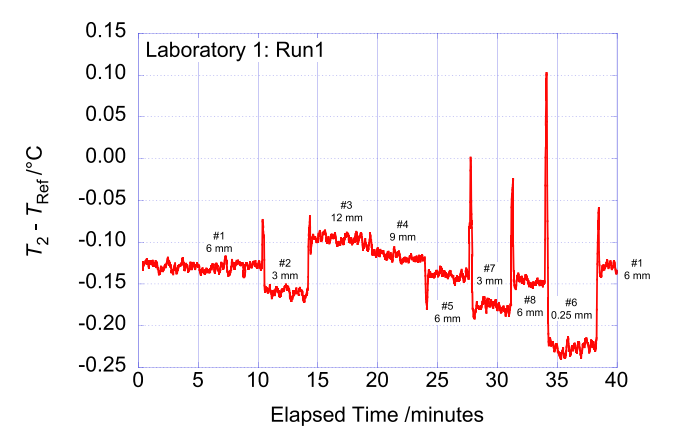


Figure 14. The data from laboratory 1 showing the difference between TC2 and the average of TC3 and TC4 in the figure. Note that the drift in all the sensors at the start of the experiment has been compensated. The differences in the reading of TC2 in the different tubes are clearly visible.

3.3.1. Laboratory 1. Figure 13 shows the four thermocouple (TC) readings taken over a 40 min period. TC1 is a 0.54 mm thermocouple permanently exposed to the air. TC2 is the probe thermocouple which is moved from tube to tube: the discontinuities on changing tube are clearly visible. TC3 and TC4 are thermocouples in the 9.6 mm and 12.8 mm tubes respectively and these are averaged to create a reference temperature.

In figure 13 it can be seen that none of the thermocouples were completely stabilised at the start of the experiment. In figure 14 we plot the difference between TC2 and the reference temperature, and it can be seen that this difference is stable at the start of the experiment.

We can extract data from figure 14 to plot the temperature changes versus the diameter of the tube. Typically, the tube temperature has a standard deviation of approximately 5 mK, and this is shown as an error bar in figure 15.

It can be seen in figure 15 that the smallest diameter under consideration produces a result which falls below the

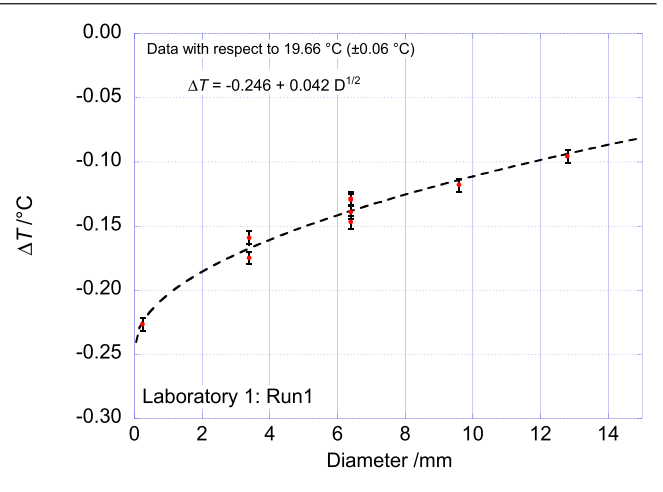


Figure 15. Analysis of the data in figure 14. The data in the plateau regions in figure 14 were extracted and their average value plotted against the tube diameter. Note that there are four readings from the 6.4 mm tubes in different places on the apparatus and two readings from the 3.4 mm tubes. The scatter amongst these points is a reasonable measure of the repeatability of results and controls for any systematic temperature change along the row of tubes. Also shown is the fit to a square root function.

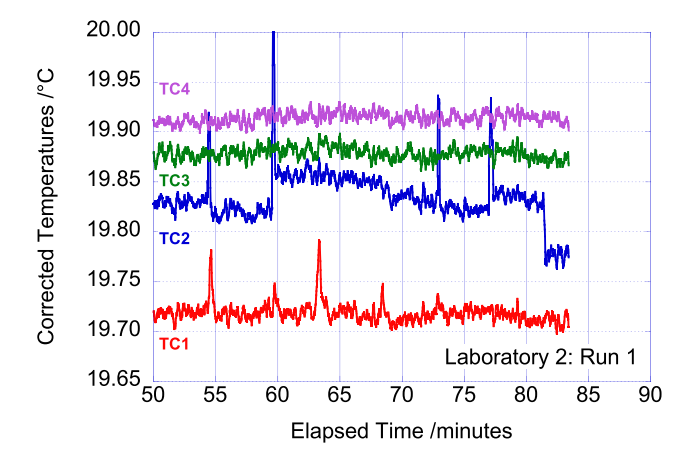


Figure 16. Data from laboratory 2 showing a 10 s running average of thermocouple readings corrected to be approximately self-consistent as described in the text. TC1 is the reading from a 0.54 mm diameter thermocouple exposed alongside the tubes. TC2 is the probe thermocouple which is moved from tube to tube. TC3 and TC4 are in the 9.6 mm and 12.8 mm diameter tubes and are used to create a reference temperature which tracks slow changes in air temperature. Of special note is the exceptional stability of this reference.

approximately linear trend of the other data and which fits well to a square root dependence on diameter. If this effect is indeed real, then it indicates that even the $0.25\,\mathrm{mm}$ thermocouple has an error of approximately 20 mK in measuring the air temperature. A 6 mm diameter sensor, such as capsule SPRT, would be in error by more than $0.1\,\mathrm{^{\circ}C}$. A second run in laboratory 1 produced closely similar results.

3.3.2. Laboratory 2. Figure 16 shows the equivalent to figure 13 for laboratory 2. The data on the difference from the reference temperature (figure 17) shows that the diameter dependence is weaker than in laboratory 1, and this is confirmed in the analysis in figure 18. This is broadly consistent

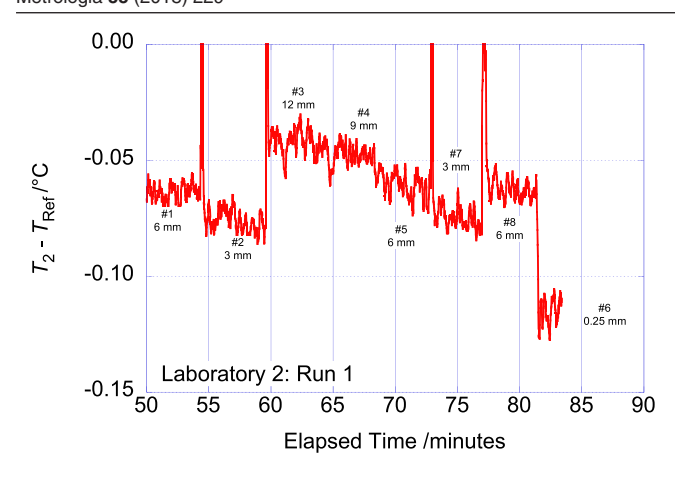


Figure 17. Data from laboratory 2 showing the difference between TC2 and the average of TC3 and TC4 in figure 16. The differences in the reading of TC2 in the different tubes are clearly visible.

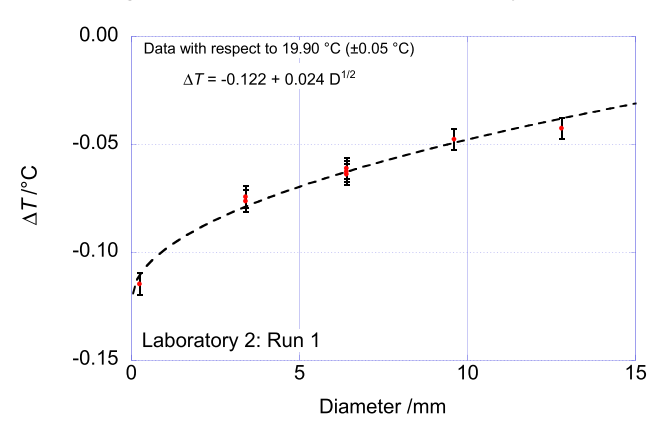


Figure 18. Analysis of the data in figure 17. The data in the plateau regions in figure 17 were extracted and their average value plotted against tube diameter. Note that there are four readings from the 6.4 mm tubes in different places on the apparatus and two readings from the 3.4 mm tubes. The scatter amongst these points is a reasonable measure of the repeatability of results and controls for any systematic temperature change along the row of tubes. Also shown is the fit to a square root function.

with the fact that (based on the readings of the thin thermocouple TC1), the air in laboratory 2 is approximately 0.4 °C warmer than laboratory 1, while the wall temperatures and illumination levels are similar.

3.4. Comparison with model

Given the large uncertainties in the sensor emissivity, and the direct and thermal irradiances, we can attach very little significance to the closeness of agreement between the model summarised in equation (13) and the data acquired in laboratories 1 and 2. Instead we seek to demonstrate two things. Firstly, that the theory is plausibly consistent with the data given reasonable estimates of the parameters, and secondly that the data do indeed show a dependence on the square root of the tube diameter.

Using the environmental parameters in table 1 we have evaluated equation (13) for the situation in the two laboratories (table 2) and these model predictions are plotted alongside the data from figures 15 and 18 in 19.

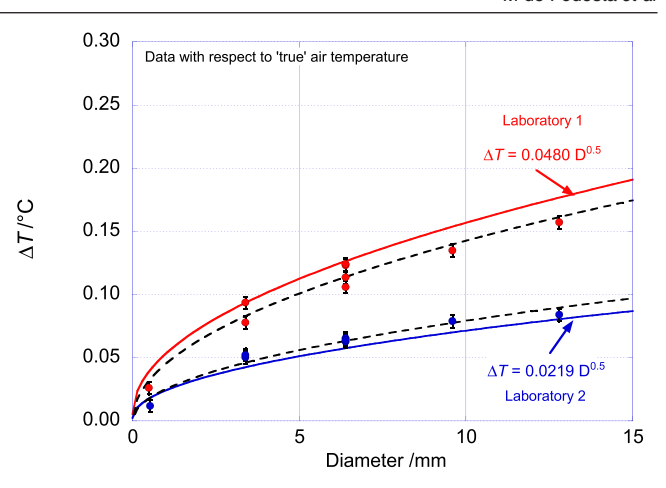


Figure 19. The continuous lines show the predicted diameter dependence of the temperature error for laboratories 1 and 2 evaluated using the parameters in table 1 with a sensor emissivity of 0.5. Also shown are the data and fits from figures 15 and 18 offset to place the estimated true air temperature at zero.

It is clear that the model and data are both plausibly described by a square root dependence on diameter *D*. We also note that using the parameters in table 1 there is a plausible agreement with the diameter dependence observed in each of the two laboratories. Given the significant uncertainties in the input parameters, the level of agreement in figure 19 and table 2 must be considered fortuitous. Nonetheless, it does demonstrate that with reasonable and unforced parameter choices, the theory outlined in section 2 can plausibly explain the diameter dependence measured in section 3.3.

3.5. Emissivity test

One weakness of the tests in the previous section is that it was not possible to verify that the surface emissivity of all the probes and tubes used was identical. The MIMS thermocouples and tubes used were all 'stainless steel', and all looked to have a qualitatively similar finish. However, we had no way to check that they did indeed have an identical surface emissivity.

To address this point, a similar set of tubes to that described in figure 13 was prepared and a set of measurements was taken using the procedure described in section 3.3. The outside diameters of the set (1.3 mm, 2.1 mm, 3.2 mm, 6.4 mm, 9.6 mm, 12.8 mm and 41 mm) included smaller and larger tubes than in the previous experiments. After this set of measurements was taken, all but two of the tubes were sprayed with matt black paint. Although the coverage and surface finish of the paint might vary from tube to tube, we can reasonably expect that their emissivity was similar. Also, we expect this paint to have a considerably higher emissivity than stainless steel, both in the optical and infrared regions of the electromagnetic spectrum.

Figure 20 shows the difference, before and after painting, between the thermocouple reading recorded in the tubes and the average reference temperature recorded in two 6.4 mm diameter tubes, which were exposed alongside the experimental tubes, but which were left unpainted. We can draw several conclusions by analysing figure 20.

Table 2. Fitted values of the offset and coefficient of the square-root term for two runs in laboratories 1 and 2. Also shown is the value of the predicted coefficient of the square-root term based on the analysis in section 3 using the environmental parameters in table 1.

	Offset (K)	Coefficient (K mm ^{-0.5})	Model (K mm ^{-0.5})
Laboratory 1: run 1 Laboratory 1: run 2	-0.246 ± 0.007 -0.245 ± 0.008	$\begin{array}{c} 0.0425 \pm 0.0030 \\ 0.0408 \pm 0.0031 \end{array}$	0.0480
Laboratory 2: run 1	-0.122 ± 0.003	0.0235 ± 0.0014	0.0219

Firstly, it is clear that the painted tubes warm more than the unpainted ones: this clearly identifies radiation as the source of the heating. Secondly, we note that both sets of data can be reasonably described as being proportional to the square root of the diameter: this clearly identifies the role of air flow in determining the final tube temperature.

Finally, we note that with respect to the reference temperature, the inferred zero-diameter temperature from the painted data is -0.126 ± 0.009 °C, and it is -0.111 ± 0.004 °C from the unpainted data. These estimates differ by only 15 mK and the uncertainty of the estimates combined in quadrature is approximately 10 mK. These differences and uncertainties are approximately ten times smaller than the error which would be incurred by making a single measurement of air temperature using an SPRT with a diameter of 6 mm. The difference between the painted and unpainted tubes at the diameters of the real thermometers and larger items shows that even in the best controlled laboratories, surface emissivity is critical to the temperature attained by a sensor or other object.

4. Discussion and recommendations

4.1. General comments

One of the reasons that Nicholas and White [5] describe radiative errors as 'insidious' is that without auxiliary measurements, there is no simple way to detect whether or not a temperature sensor is being affected by a radiative load. The low heat capacity of the air makes air temperature sensors especially susceptible to radiative errors, particularly in slow-moving air. As a consequence, almost every air temperature measurement made—even in well-controlled environments—is subject to radiative errors of unknown magnitude.

However, there is a simple way to detect and correct for radiative errors in air temperature measurements by taking measurements using two or more sensors with similar surface emissivity, but different diameters (figure 20). For a wide range of sensor sizes and air speeds, the radiative error is expected to be proportional to the square root of the sensor diameter. So for two sensors with diameters D_1 and D_2 reading temperatures T_1 and T_2 , the air temperature can be estimated by:

$$T_{\text{Air}} = \frac{T_1 - T_2 \left[\frac{D_1}{D_2}\right]^{\frac{1}{2}}}{1 - \left[\frac{D_1}{D_2}\right]^{\frac{1}{2}}}.$$
 (17)

For the special case of two sensors with diameters differing by a factor 4, the larger sensor should display twice the error of the smaller sensor, and the air temperature can be estimated simply as $T_{Air} = 2T_1 - T_2$. When the air temperature is changing, it

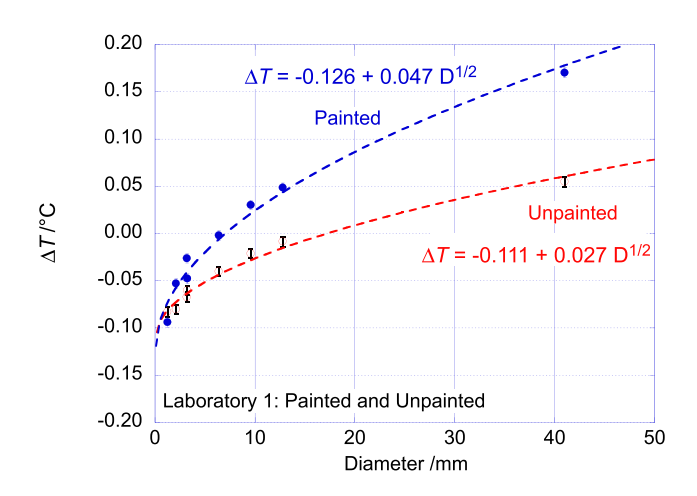


Figure 20. Measurements of the temperature recorded in tubes of different diameters with respect to the average temperature in two 6.4 mm diameter tubes which were left unpainted. Painting the tubes black results in greater temperature deviations, but extrapolation using a function proportional to the square root of the sensor diameter results in an estimate free from radiative effects with an uncertainty of approximately 15 mK.

is important to use sensors with equal heat capacity in order to balance their dynamic response. Alternatively, instruments such as the *Radiation Compensating Thermocouple* [3] could be resurrected for the modern era.

4.2. Dimensional measurements

One consequence of the arguments outlined above is that the radiative environment in the closely controlled laboratories at NPL is such that an air flow of $\sim 0.11~{\rm m~s^{-1}}$ is insufficient to effectively cool objects larger than a fraction of a millimetre in diameter. Large objects within the room are radiatively coupled to the lights, walls, ceiling and floor much more strongly than they are thermally coupled to the air.

As a consequence, the objects in these rooms cannot be guaranteed to be at the temperature of the thermometers placed near to them. The highest level measurements require the temperature of an artefact to be known with uncertainties on the order of 1 mK. This can be achieved by either using dummy artefacts with an embedded contact temperature sensor, or, more dauntingly, by using a thermal model which accounts for the object's size and shape, the true air temperature and flow speed and the optical and thermal radiation intensities to which it is exposed.

The true air temperature (which determines the refractive index of the air) is likely to be lower than the air temperature indicated by any contact thermometer. However, 'thin and shiny' thermometers, i.e. those with a low emissivity surface,

are likely to give a better estimate than 'thick and dark' thermometers. Even in these well-controlled environments, errors exceeding 0.1 °C are possible.

Additionally, strategies such as enclosing a laser beam within a tube to reduce the effects of air turbulence, can potentially introduce systematic errors if the air temperature is not measured *within* the tube. Similarly, the 'radiation shielding' recommended in [5] could easily produce additional errors since the shield may create an unrepresentative micro-climate within it.

Where the lowest uncertainties are required and radiative effects are found to be significant by investigating the diameter-dependence of apparent air temperature, there are many strategies that can be used to estimate the true air temperature.

If using PRTs, it is advisable to use the thinnest, lowest emissivity version available. In general, the highest quality PRTs (SPRTs) are only available in capsule form with a diameter of typically 6mm. However, in this application, where the sensors are unlikely to undergo temperature excursions beyond a few degrees away from room temperature, a thinner PRT—and they are available with diameters as small as 0.5 mm—will suffer least radiative error, while still being able to display acceptable repeatability. When used with low measuring currents, such probes will show smaller radiative errors than more conventional 3 mm diameter and 6 mm diameter probes.

Although using PRTs to measure the temperature of solid objects will result in the lowest uncertainty in principle, there might be advantages in measuring air temperature using thermocouples. These are available in thinner formats than PRTs and the loss of sensitivity may be compensated by the reduction in uncertainty due to small radiative loading and the absence of self-heating.

The reason that such a replacement is feasible is because the thermocouples would only be used close to 20 °C, and can be made uniquely thin: 0.25 mm is possible for thermocouples sheathed in stainless steel. They can also be polished for even lower radiative errors. If this procedure was adopted, the coldjunction should be carefully designed and measured using a PRT or thermistor measurement system. Since the basic sensitivity of type K thermocouples is approximately 40 μ V °C⁻¹, the use of a sensitive digital voltmeter should result in measurement uncertainties of the order of 0.01 °C with no selfheating and the smallest radiative errors. Outstanding work on this approach has been carried out by Nicolaus *et al* at PTB [26, 27].

A final alternative might involve use of bare glass-encapsulated thermistors, which would have higher temperature sensitivity than a PRT or thermocouple, and being roughly spherical, they would have a higher heat transfer coefficient than a cylinder of equal diameter (figure 9). Ideally the sensor would be silvered for even lower errors.

No matter which sensor is chosen, the true air temperature can be estimated by using a multi-sensor technique.

4.3. Mass metrology

Air temperature is a critical measurement in mass metrology because of the requirement to assess the buoyancy of the objects being weighed. However, the design philosophy adopted to create a stable environment in mass labs is usually quite different from that employed in dimensional laboratories. Instead of having powerful air conditioning and laminar flow, the laboratories typically have a lower air flow (~0.05 m s⁻¹ or less) and objects are allowed to stabilise passively; the weighings are thus carried out in air which is very nearly static.

Temperature measurements are made *within* a balance enclosure which is screened from drafts. We have not investigated this situation in detail but note that the measurement of air temperature using sensors within the balance enclosure may be exquisitely sensitive to small radiant loads because of the extremely low air flow. For example, if the air flow was 0.01 m s⁻¹, an irradiance of 10 W m⁻²—similar to that in dimensional laboratories (table 1)—on a 3 mm diameter PRT with an emissivity of 0.5 would result in a temperature error of approximately 0.16 °C.

Once again, the use of multiple sensors of different diameters is recommended to assess the magnitude of the effect, and a *Radiation Compensating Thermocouple* [3]—or modern equivalent—may prove convenient.

4.4. Precision measurement in general

It is likely that the insights in this paper offer many opportunities for improving air temperature measurements carried out either within close-control laboratories or climatic chambers. Typically, measurements and calibrations carried out in these environments support mass and dimensional studies, but may have an impact on other fields such as gas analysis, humidity and potentially radiometry or ionising radiation measurements.

One area of special concern is where two thermometers are compared during calibration. Heinonen [11] has already highlighted the problem of sensors with different emissivities, but this work shows that differences in sensor diameters can also lead to errors where a thin sensor 'inherits' the larger radiation error from a larger calibrated sensor.

The use of multiple sensors with different diameters provides a way of assessing the magnitude of the radiative errors, and in the near term this may be the most appropriate way to proceed. But in the longer term, acoustic thermometry, which measures the average temperature and humidity using a noncontact technique, may well give better results than any of the techniques mentioned above since it returns an average over a significant volume of laboratory air and should be less affected by radiative effects [1, 2]. It may also be possible to deduce the average temperature along the beam path of a laser interferometer.

4.5. Meteorology

4.5.1. Thermometer screens. That meteorological air temperature sensors are subject to radiative errors at low wind speeds is well known. However, without associating a wind speed measurement to a temperature measurement, it is still difficult to diagnose precisely when a sensor is being affected by radiative errors and by how much.

We do not know why the *Radiation Compensated Thermocouple* [3]—or a descendent of it—is not widely used in meteorology. But the absence of an equivalent instrument means that radiative errors are ubiquitous in meteorological measurements. Subject to the caveat that any changes in meteorological observing practice should be implemented with a period of overlap to allow the assessment of systematic changes, it is possible that small changes in observing practice could result in a considerable improvement in the current situation.

Firstly, small or thin sensors with shiny surfaces are less affected than larger diameter sensors. This is already recognised in the recommendation in the CIMO guide [19]. However, the insight could be applied to sensors within screens as well as to sensors exposed directly to sunlight. For sensors with an emissivity of 0.5, a screen which is 3 °C warmer than the air in a wind speed of 0.1 m s⁻¹ will result in \sim 0.5 °C error for a 6 mm diameter sensor but only \sim 0.2 °C error for a 1 mm diameter sensor. Any reduction in sensor surface emissivity will reduce the error almost proportionately.

Secondly, the radiative error in a wide range of circumstances is expected to vary as the square root of the sensor diameter, and even 1 mm diameter sensors can still have significant errors. This fact suggests—as described in section 4.1—the use of dual sensors with different diameters, where the difference in reading between sensors is used to infer the reading of a hypothetical 'zero diameter' sensor. For remote exposures with limited access to electrical power, this has the advantage of requiring less power than using an aspirated sensor.

4.5.2. Aspirated sensors. Aspirated thermometer housings, in which air is drawn continuously through a screen, are generally accepted [28] as giving the lowest uncertainty in meteorological air temperature measurements. With such screens, airflows of several metres per second are typical and it is generally considered that faster air flows give reduced errors. The insights from this work now suggest two ways to improve such measurements.

Firstly, as suggested by Bugbee [24, 25] using smaller sensors will—subject to self-heating corrections—reduce radiative errors significantly. It may be that this reduction in uncertainty satisfies meteorological requirements entirely. However, a second approach might be to make estimates of the magnitude of the radiative error. This could be estimated from measurements of temperature reading versus air speed—with the variation achieved by varying the fan speed. Alternatively this could be estimated by using two sensors with differing diameters in the same air flow.

4.5.3. Radiosonde measurements. Much of the early work referenced in this paper was undertaken in order to make reliable measurements in the challenging environment of the upper atmosphere [16]. The legacy of that work is the now routine use of radiosondes to make temperature measurements in the upper atmosphere with only small radiant errors [29, 30]. Using a standard model of the atmosphere, the heat transfer coefficient for a wire sensor is approximately seven times smaller at an altitude of 18 km compared with its value at ground level, and irradiance in excess of 1000 W m⁻² is possible. Despite this, uncertainties below 1 °C are possible by careful estimation of the pressure- and wind-speed dependence of the error [31]. Additionally, the small size of the thermistors, resistors and capacitance sensors (see figure 1 in [31]), together with their highly reflective coating with an estimated emissivity of 0.02, contributes to the small radiative

Reflecting on this achievement, it seems likely that the technologies already adopted for air temperature measurement in radiosondes may find future applications in terrestrial environments in which low radiant errors are required. Additionally, the introduction of multiple temperature sensors with different diameters on radiosondes could allow the estimation of the radiant load and correction for the small residual radiative error.

4.5.4. Climate reference networks. The 'sensor size' effect is highly relevant to applications where the greatest care is taken to first reduce and then properly characterise measurement biases. Thus this work may well have specific relevance to extant and future attempts to create reference networks of meteorological stations, specifically the US Climate Reference Network [28], the GCOS Reference Upper Air Network [29] and the ESA Fiducial Reference Measurements programme.

4.6. Further work

This paper is inevitably incomplete. Its bibliography could be substantially improved and there are many more and better calculations to be made regarding the air flow in different directions across sensors, as well as across surfaces and other geometrical shapes relevant to advanced metrology. Furthermore, there are many better measurements that could be made. We hope to address some of these points in future publications.

However, we hope that the most significant impact of this paper will be in the development of practical procedures for detecting radiative errors, estimating their magnitude, and finally minimising their impact. This is especially important for metrological work in which an uncertainty in air temperature of less than u(k = 1) = 0.1 °C is required, or in which the temperature of objects must be controlled using flowing air, either within a climatic chamber or in an open laboratory.

In meteorology, procedures are already in place to deal with radiative errors, which are ubiquitous. However, the work described here may help to establish when data are subject to

such errors, and help evaluate the magnitude of the effect. In the future, instruments may also be developed which are substantially immune to the effect.

In the longer term, in both metrological and meteorological applications, there may well be advantages to developing non-contact thermometry in air, for example by acoustic or optical methods. Although complex, these techniques are likely to be relatively immune to radiation errors, and appreciation of the significance of such errors in contact thermometers may well tip the balance of practicality in favour of non-contact solutions.

Acknowledgments

The authors would like to thank their colleagues who helped with this work specifically: Peng Miao, Andrew Lewis, Sheryl Bailey, Tim Coveney and visiting student William Severn. Also, Gordon Edwards for a thorough examination of the manuscript. Additionally the authors are grateful for the advice from Victor Venema, Stephen Burt, Rod White and Ross Mason. This work was partly funded by the UK Department for Business, Energy and Industrial Strategy and also by the European Metrology Research Program (EMRP) through the METEOMET and METEOMET2 projects. The EMRP is jointly funded by the EMRP participating countries within EURAMET and the European Union.

ORCID iDs

Michael de Podesta https://orcid.org/0000-0002-6635-6806

References

- [1] Underwood R, Gardiner T, Finlayson A, Few J, Wilkinson J, Bell S, Merrison J, Iverson J J and de Podesta M 2015 A combined non-contact acoustic thermometer and infrared hygrometer for atmospheric measurements *Met. Apps* 22 830–5
- [2] Underwood R, Gardiner T, Finlayson A, Bell S and de Podesta M 2017 An improved non-contact thermometer and hygrometer with rapid response *Metrologia* 54 S9
- [3] Daniels G E 1968 Measurement of gas temperature and the radiation compensating thermocouple *J. Appl. Meteorol.* 7 1026–35
- [4] Harrison R G 2015 Meteorological Measurements and Instrumentation (New York: Wiley)
- [5] Nicholas J V and White D R 1991 Traceable Temperatures 2nd edn (New York: Wiley)
- [6] Quinn T 1990 Temperature 2nd edn (New York: Academic)
- [7] Bentley R E 1998 Temperature and Humidity Measurement (Berlin: Springer)
- [8] ASTM 1993 Manual on the Use of Thermocouples in Temperature Measurement (Philadelphia, PA: ASTM)
- [9] Bentley R E 1998 Theory and Practice of Thermocouple Thermometry (Berlin: Springer)

[10] Michalski L, Eckersdorf K and McGhee J 1991 Temperature Measurement 1st edn (New York: Wiley)

- [11] Heinonen M et al 2014 Int. J. Thermophys. 35 1251
- [12] Friederici S and Tegeler E 2004 Proc. of TEMPMEKO 2004, 9th Int. Symp. on Temperature and Thermal Measurements in Industry and Science ed D Zvizdić et al (Zagreb: FSB/ LPM) pp 795–800
- [13] Incropera F P and De Witt D P 2011 Fundamentals of Heat and Mass Transfer (New York: Wiley)
- [14] Çengal Y A and Ghajar A J 2015 Heat and Mass Transfer: Fundamentals and Application 5th edn (New York: McGraw-Hill)
- [15] Burt S 2012 The Weather Observer's Handbook (Cambridge: Cambridge University Press)
- [16] Ney E P, Maas R W and Huch W F 1960 The measurement of atmospheric temperature J. Meteorol. 18 60–80
- [17] Wells W C 1815 Essay on dew, constable 150pp
- [18] Waggener W J 1898 Über die Messung von Flammentemperturen durch Thermoelemente, insbesondere über die Temperaturen in Bunsen' schen Blaubrenner (On the measurement of flame tempertures by thermocouples, in particular about the temperatures in Bunsen's burners) *Verhandl. Physik. Ges.* **14** 78–83
- [19] CIMO 2014 Measurement of Temperature CIMO Guide to Meteorological Instruments and Methods of Observation (Geneva, Switzerland: World Meteorological Organization) ch 2
- [20] Erell E, Leal V and Maldonado E 2005 Measurement of air temperature in the presence of a large radiant flux: an assessment of passively ventilated thermometer screens *Bound. Layer Meteorol.* 114 205–31
- [21] Harrison R G and Pedder M A 2001 Fine wire thermometer for air temperature measurement *Rev. Sci. Instrum.* 72 1539
- [22] Harrison R G and Rogers G W 2006 Fine wire thermometer amplifier for atmospheric measurements *Rev. Sci. Instrum.* 77, 116112
- [23] Harrison R G 2010 Natural ventilation effects on temperatures within Stevenson screens Q. J. R. Meteorol. Soc. 136 253–9
- [24] Bugbee B 2015 Private Communication and presentation at Meteorological World Expo 2015, Brussels
- [25] Bugbee B, Monje O and Tanner B 1996 Quantifying energy and mass transfer in crop canopies Adv. Space Res. 18 149–56
- [26] Nicolaus A, Bartl G, Peter A, Kuhn E and Mai T 2017 Volume determination of two spheres of the new ²⁸Si crystal of PTB Metrologia 54 512–5
- [27] Arnold Nicolaus R and Geckeler R D 2007 Improving the measurements of the diameter of Si spheres *IEEE Trans*. *Instrum. Meas.* 56 517–22
- [28] Diamond H J et al 2013 US Climate Reference Network after one decade of operations: status and assessment Bull. Am. Meteorol. Soc. 94 489–98
- [29] Dirksen R J, Sommer M, Immler F J, Hurst D F, Kivi R and Vömel H 2014 Reference quality upper-air measurements: GRUAN data processing for the Vaisala RS92 radiosonde Atmos. Meas. Technol. 7 4463–90
- [30] CIMO 2014 Measurement of upper-air pressure, temperature, humidity CIMO Guide to Meteorological Instruments and Methods of Observation (Geneva, Switzerland: World Meteorological Organization) ch 12
- [31] Luers J K 1997 Temperature error of the Vaisala RS90 Radiosonde *J. Atmos. Ocean. Technol.* **14** 1520–32